JME

Journal of Mining & Environment,
Vol.6, No.1, 2015, 73-93.

A boundary element analysis of crack-propagation mechanism of micro-cracks in rock-like specimens under a uniform normal tension

H. Haeri[1*], A. R. Khaloo[2], K. Shahriar[3], M. Fatehi Marji[4] and P. Moaref Vand[3]

1. Postdoctoral Fellow in Civil Engineering, Department of Civil Engineering, Sharif University of Technology, Member of National Elites Foundation, Tehran, Iran
2. Head of Center of Excellence in Structure and Earthquake Engineering, Sharif University of Technology, Tehran, Iran
3. Department of Mining and Metallurgical Engineering, Amirkabir University of Technology, Tehran, Iran
4. Faculty of Mining and Metallurgy, Institution of Engineering, Yazd University, Yazd, Iran

Received 3 August 2013; received in revised form 12 February 2015; accepted 22 February 2015
**Corresponding author: haerihadi@gmail.com (H. Haeri).*

Abstract
In this work, the mechanism for fracture of brittle substances such as rocks under a uniform normal tension is considered. The oriented straight micro-cracks are mostly created in all the polycrystalline materials resulting from the stress concentrations. The present work focuses on the interactions of the pre-existing micro-cracks, which can grow and propagate within a rock-like specimen. The micro-crack initiation and propagation in rock-like specimens is investigated using the Fortran Code TDDCRACK^{2D}, which is a 2D displacement discontinuity method (DDM) for crack analysis, a boundary element computer code based on the linear elastic fracture mechanics (LEFM) theory. In the present work, a higher order DDM is used to implement special crack tip elements for estimation of the stress intensity factors (SIFs) and crack initiation angles for the wing-crack problems initiated at different angles from the original micro-crack tips in an infinite specimen under a uniform tension.

Keywords: Micro-Cracks, crack Interaction, crack Initiation, Rock-Like Specimens, Linear Elastic Fracture Mechanics (LEFM) Theory, Displacement Discontinuity Method (DDM), Crack Coalescence.

1. Introduction

The crack propagation mechanism for solid materials can be divided into two scales: micro-fracture that usually deals with the initiation and propagation of micro-cracks, and macro-fracture that deals with the propagation of big cracks. One can find to what extent the macro-fracturing mechanism is affected by the micro-fracturing one. The presence of micro-cracks in brittle substances has more effects on their mechanical behaviors. The mechanical behavior of rocks is due to their micro-mechanical structures [1]. Micro-cracks typically nucleate at the positions of stress concentrations such as pores, inclusions, sharp micro-cracks, and triple connections. Initiation of a micro-crack also occurs at the micro-crack tip, and extends at an angle with respect to the original micro-crack plane [2]. The resulted cracks may be further extended in kinked or curved forms. [3]. In uniaxial tension loadings, crack initiation and specimen fracture may happen very soon.

The mechanism for fracture of brittle substances with orientated micro-cracks depends upon the degree of interaction between the micro-cracks and coalescence path, leading to a crack in the macro-scale [4]. In studying the fracture mechanism of brittle substances under uniaxial tensile stress, fracture initiation is normally expected in a direction perpendicular to the maximum tensile stress, i.e. in the plane of the critically oriented micro-cracks. In the case of brittle fracture under compressive loading, one might therefore expect that fracture initiation also follows in a direction parallel to the maximum compression stress, i.e. the one which is inclined at 20-30° to the maximum stress direction [5]. In rocks, crack initiation under tensions tress is preferred due to the lower toughness of rock

substances in tension than in shear [6]. The mechanism of forming and coalescing micro-cracks in composing macro-cracks (fatal-cracks) or rupture of rocks is yet not a well-understood matter, and the problem of the interaction between micro-cracks and macro-cracks is always noted by the researchers [7]. Although a number of experimental reports have been published on the micro-crack and coalescence patterns of specimens such as single and three micro-cracks under uniaxial and biaxial compression loadings[e.g. 8-20], the extension numerical models such as the code FROCK, damage model, rock failure process analysis ($RFPA^{2D}$), and2D particle flow code (PFC^{2D}) are used in this field [6, 10, 12, 13, 21-29]. A comparison between the results obtained for several numerical models and those obtained for the experiments conducted by Bobet-Einstein and Sagong-Bobet [12, 13, 16] are in good agreement. Due to the complexity of the problem, nowadays, numerical or analytical-numerical approaches are mostly used for the rock-fracture modeling mechanism [7]. A researcher analyses the growth of micro-cracks in infinite planes. The present investigation was carried out on the effect of fracturing on brittle substances altering positions of micro-cracks that are under tension loadings. A numerical model, the displacement discontinuity crack ($TDDCRACK^{2D}$) code, and a 2D code based on the linear elastic fracture mechanics (LEFM) theory were used to simulate the micro-crack interaction of specimens containing micro-cracks. There are a number of important fracture initiation criteria that are applicable in practice, as follow: the maximum tangential stress (σ_θ-criterion), the maximum energy release rate (G-criterion),the minimum energy density criterion (S-criterion),and any modified form of these mentioned issues e.g. F-criterion, which is a modified energy release rate criterion [11, 30-36]. Although these criteria act prosperously for predicting the wing-crack initiation (tension-crack) under tension and compression loadings, the maximum tangential stress criterion was used here to predict the direction of micro-crack initiations. In the present work, the numerical analysis of the growth of wing-cracks from the pre-existing micro-cracks in rock-like specimens under a uniform normal tensile stress was studied. The initiation and growth of wing-cracks from a single micro-crack (like the center slant micro-crack) were solved, firstly, by the proposed numerical model to verify the results obtained using the higher order displacement discontinuity code $TDDCRACK^{2D}$, which uses the linear and quadratic displacement discontinuity formulation with three special crack tip elements at each micro-crack end. Comparing the numerical and analytical values for the fracture parameters like mode I and mode II, the stress intensity factors (SIFs)were calculated for the problems, and the validity of the numerical results was proved. These results also show high accuracy of the numerical values obtained by the proposed method. Then the extension and growth of each micro-crack and the interaction between them were studied. In all cases, plane stress was used to solve the stresses and displacements.

2. Application of quadratic collocation displacement discontinuity method (DDM) using three special crack tip elements

In the displacement discontinuity method (DDM), the micro-crack surfaces are divided into multiple segment elements, and for each one of these elements, the opening displacement D_y (normal displacement discontinuity) and the sliding displacement D_x (shear displacement discontinuity) are directly calculated. Considering a displacement discontinuity element with the length of 2c on the x-axis, the widespread displacement discontinuity variable $u(\zeta)$ can be calculated (Figure 1a). D_x and D_y are easily determined by taking the u_x and u_y components of the widespread displacement discontinuity variable $u(\zeta)$ in the interval [-c, +c], as shown in Figure 1b.Therefore, the fundamental variables D_x and D_y can be written as [37, 38]:

$$\begin{aligned} D_x &= u_x(x,0_-) - u_x(x,0_+) \\ D_y &= u_y(x,0_-) - u_y(x,0_+) \end{aligned} \quad (1)$$

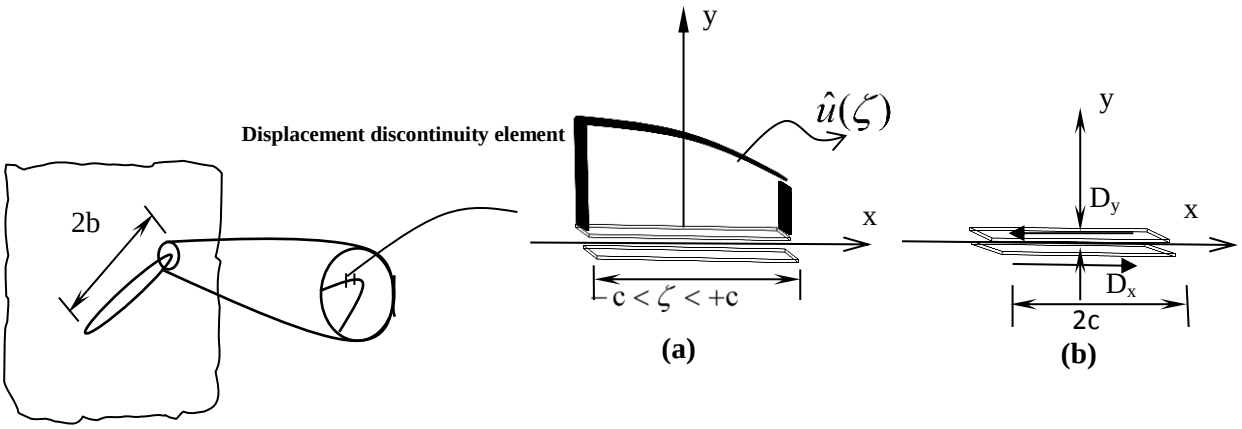

Figure 1. (a) Displacement discontinuity element and widespread displacement discontinuity variable u(ζ), (b) constant element displacement discontinuity.

In DDM, the boundaries are discretized into multiple segment elements. The formulations of three types of displacement discontinuity variations with a constant variation in the displacement along the elements, a linear variation, and a quadratic variation have been previously mentioned and used in the literature [38-40]. The quadratic collocation displacement discontinuity is fundamentally based upon integrating the quadratic collocation shape functions over the collinear, straight-line displacement discontinuity elements.

Figure 2 shows the displacement distributions at the quadratic collocation point 'm', which can be calculated as:

$$D_j(\zeta) = \sum A_m(\zeta) D_j^m \quad for \quad m = 1,to\,3,\ j = x, y \tag{2}$$

where D_j is the fundamental variable. In each collocation point, two fundamental variables are calculated. Using $c_1 = c_2 = c_3$, we have:

$$A_1(\varepsilon) = \zeta(\zeta - 2c_1)/8{c_1}^2,\ A_2(\zeta) = -(\zeta^2 - 4{c_1}^2)/4{c_1}^2,\ A_3(\zeta) = \zeta(\zeta + 2c_1)/8{c_1}^2 \tag{3}$$

which are the shape functions of the quadratic collocation point 'm'. In the quadratic collocation, there are three collocation points for each element, in which the displacements are typically calculated. These collocations are located in the center of the elements (Figure 2).

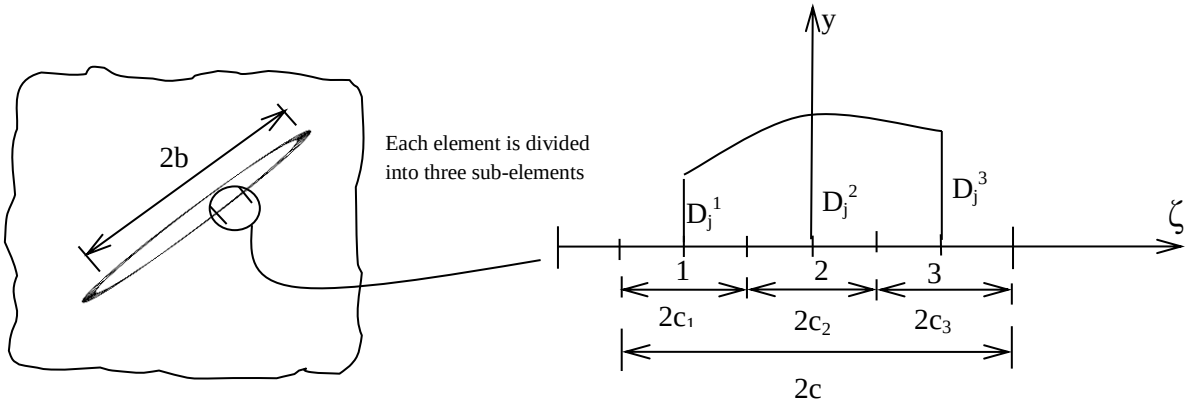

Figure 2. Quadratic collocations for higher order displacement discontinuity variation.

The stresses and displacements for an oriented straight micro-crack in an infinite specimen along the *x-axis* in terms of the single harmonic functions N(y,x) and M(y,x)have been given by Crouch and Starfield [38] as:

$$\begin{aligned}
\sigma_{xx} &= 2\rho\left[2N_{xy} + yN_{xyy}\right] + 2\rho\left[M_{yy} + yM_{yyy}\right] \\
\sigma_{yy} &= 2\rho\left[-yN_{xyy}\right] + 2\rho\left[M_{yy} - yM_{yyy}\right] \\
\sigma_{xy} &= 2\rho\left[2N_{yy} + yN_{yyy}\right] + 2\rho\left[-yM_{xyy}\right]
\end{aligned} \tag{4}$$

and the displacements are:

$$\begin{aligned}
u_x &= \left[2(1-\nu)N_y - yN_{xx}\right] + \left[-(1-2\nu)_x - yM_{xy}\right] \\
u_y &= \left[(1-2\nu)N_x - yN_{xy}\right] + \left[2(1-\nu)M_y - yM_{yy}\right]
\end{aligned} \tag{5}$$

ρ is the shear modulus, and N_y, M_y, N_x, and M_x, are the partial derivatives of the single harmonic functions N(y,x) and M(y,x) with respect to y and x. These potential functions (for a quadratic variation of displacement discontinuity along the element) [40] can be written as:

$$N(x,y)=\frac{-1}{4\pi(1-\nu)}\sum_{m=1}^{4}D_x^m\Omega_k(I_0,I_1,I_2)\ ,\quad M(x,y)=\frac{-1}{4\pi(1-\nu)}\sum_{m=1}^{4}D_y^m\Omega_k(I_0,I_1,I_2) \tag{6}$$

The common function Ω_k can be defined as:

$$\Omega_k(I_0,I_1,I_2)=\int N_k(\zeta)\ln\left[(x-\zeta)+y^2\right]^{\frac{1}{2}}d\zeta,\quad \text{k}=1,\text{to}\,3 \tag{7}$$

The integrals I_0, I_1, and I_2 in function (7) can be obtained as:

$$I_0(x,y)=\int_{-c}^{c}\ln\left[(x-\zeta)^2+y^2\right]^{\frac{1}{2}}d\zeta=y(\theta_1-\theta_2)-(x-c)\ln(\Gamma_1)+(x+c)\ln(\Gamma_2)-2c \tag{8-a}$$

$$I_1(x,y)=\int_{-c}^{c}\zeta\ln\left[(x-\zeta)^2+y^2\right]^{\frac{1}{2}}d\zeta=xy(\theta_1-\theta_2)+0.5\left(y^2-x^2+c^2\right)\ln\frac{\Gamma_1}{\Gamma_2}-cx \tag{8-b}$$

$$I_2(x,y)=\int_{-c}^{c}\zeta^2\ln\left[(x-\zeta)^2+y^2\right]^{\frac{1}{2}}d\zeta=\frac{y}{3}(3x^2-y^2)(\theta_1-\theta_2)+$$
$$\frac{1}{3}(3xy^2-x^3+c^3)\ln(\Gamma_1)-\frac{1}{3}(3xy^2-x^3-c^3)\ln(\Gamma_2)-\frac{2c}{3}(x^2-y^2+\frac{c^2}{3}) \tag{8-c}$$

where θ_1, θ_2, Γ_1, and Γ_2 can be derived as:

$$\theta_1=\arctan(\frac{y}{x-c}),\ \theta_2=\arctan(\frac{y}{x+c}),\Gamma_1=\left[(x-c)^2+y^2\right]^{\frac{1}{2}}\text{ and }\ \Gamma_2=\left[(x+c)^2+y^2\right]^{\frac{1}{2}} \tag{9}$$

Partial derivatives of the integrals I_0, I_1, and I_3 required for the solution of finite, infinite plane problems are given in the appendix.

In order to eliminate the singularity of the displacements and stress calculation near the micro-crack ends, and to increase the accuracy of the higher order DDM around the original micro-crack tip, a special treatment of the micro-crack at the tip is necessary [29, 30, 38]. In the previous works, usually, one or two elements for a specific crack tip has (have) been used. However, in the present work, three special crack tip elements were used at the end and initiation of each micro-crack in the general higher order DDM. As shown in Figure 3, using a special crack tip element with the length of 2c, the displacement discontinuity variations along this element can be written as the following form [40]:

$$D_j(\zeta)=T_1\zeta^{\frac{1}{2}}+T_2\zeta^{\frac{3}{2}}+T_3\zeta^{\frac{5}{2}} \tag{10}$$

Equation (10) can be arranged as the following form:

$$D_j(\zeta)=[A_{T1}(\zeta)]D_j^1(c)+[A_{T2}(\zeta)]D_j^2(c)+[A_{T3}(\zeta)]D_j^3(c) \tag{11}$$

The crack tip element has the length $c=c_3+c_2+c_1$. Considering $c_1=c_2=c_3$, the shape functions $A_{T1}(\zeta)$, $A_{T2}(\zeta)$ and $A_{T3}(\zeta)$ can be written as:

$$A_{T1}(\zeta)=\frac{15\zeta^{\frac{1}{2}}}{8c_1^{\frac{1}{2}}}-\frac{\zeta^{\frac{3}{2}}}{c_1^{\frac{3}{2}}}+\frac{\zeta^{\frac{5}{2}}}{8c_1^{\frac{5}{2}}},$$
$$A_{T2}(\zeta)=\frac{-5\zeta^{\frac{1}{2}}}{4\sqrt{3}c_1^{\frac{1}{2}}}+\frac{3\zeta^{\frac{3}{2}}}{2\sqrt{3}c_1^{\frac{3}{2}}}-\frac{\zeta^{\frac{5}{2}}}{4\sqrt{3}c_1^{\frac{5}{2}}}\quad\text{and} \tag{12}$$
$$A_{T3}(\zeta)=\frac{3\zeta^{\frac{1}{2}}}{8\sqrt{5}c_1^{\frac{1}{2}}}-\frac{\zeta^{\frac{3}{2}}}{2\sqrt{5}c_1^{\frac{3}{2}}}+\frac{\zeta^{\frac{5}{2}}}{8\sqrt{5}c_1^{\frac{5}{2}}}$$

The common function $\Omega_{Tm}(I_{T1},I_{T2},I_{T3})$ is defined as:

$$\Omega_{Tm}(I_{Tm})=\int_{-c}^{c}A_{Tm}(\zeta)\ln\left[(x-\zeta)^2+y^2\right]^{\frac{1}{2}}d\zeta,\ \text{m}=1,2,\text{and}\,3 \tag{13}$$

The integrals I_{T1}, I_{T2}, and I_{T3} can be expressed as:

$$I_{T1}(x,y)=\int_{-c}^{c}\zeta^{\frac{1}{2}}\ln\left[(x-\zeta)^2+y^2\right]^{\frac{1}{2}}d\zeta,$$
$$I_{T2}(x,y)=\int_{-c}^{c}\zeta^{\frac{3}{2}}\ln\left[(x-\zeta)^2+y^2\right]^{\frac{1}{2}}d\zeta \tag{14}$$
$$I_{T3}(x,y)=\int_{-c}^{c}\zeta^{\frac{5}{2}}\ln\left[(x-\zeta)^2+y^2\right]^{\frac{1}{2}}d\zeta$$

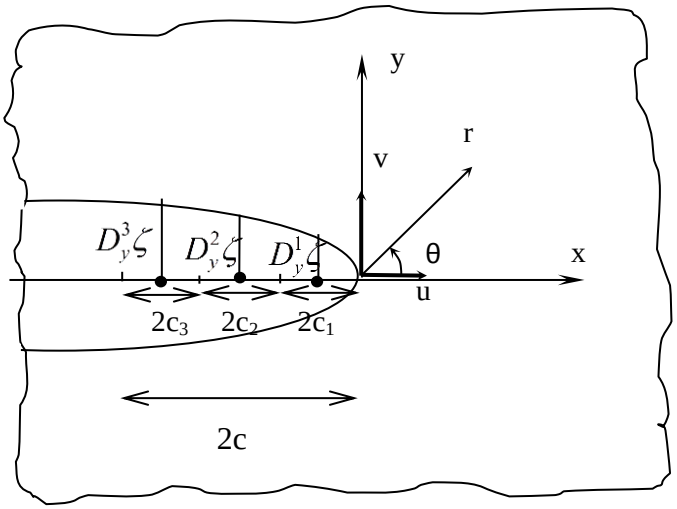

Figure 3. A special crack tip element with three equal sub-elements.

The mode I and mode II SIFs k_I and k_{II} can be estimated based on the LEFM theory as the opening and sliding displacements [39]:

$$K_I = \frac{\rho}{4(1-\nu)}\left(\frac{2\pi}{c}\right)^{\frac{1}{2}} D_y(c), \quad \text{and} \quad K_{II} = \frac{\rho}{4(1-\nu)}\left(\frac{2\pi}{c}\right)^{\frac{1}{2}} D_x(c) \tag{15}$$

3. Initiation of micro-crack under a uniform normal tension

In uniaxial tension loading, crack initiation and specimen fracture befall very soon. In the study of fracture of a brittle substance under a uniform normal tension, initiation of fracture is expected to occur in the perpendicular direction of maximum tension, and crack initiation is expected to result from the low fracture toughness in comparison to the shear loading. Generally, two types of cracks propagate from the pre-existing micro-cracks: wing-cracks and secondary-cracks (Figure 4). Wing-cracks are tension-cracks that are initiated near the original tips of micro-cracks, and stably propagate in the perpendicular direction of maximum tension. Secondary-cracks are shear-cracks that are initiated from the original tips of micro-cracks, and are stably propagated. Shear-cracks are initiated in two different directions: coplanar (quasi-coplanar) and oblique to the pre-existing micro-cracks. Two types of secondary-cracks that may simultaneously befall can be observed in Figure 4.Secondary-cracks (shear-cracks) are mostly produced under the compressive loading conditions. That is why, in this work, the focus is on the wing-cracks, and shear-cracks are not considered [22]. Wing-cracks take place when the pre-existing micro-crack inclination angle is between 30° and 90° with respect to the loading direction. Wing-cracks do not take place when the pre-existing micro-crack inclination angle is less than 30° horizontally.

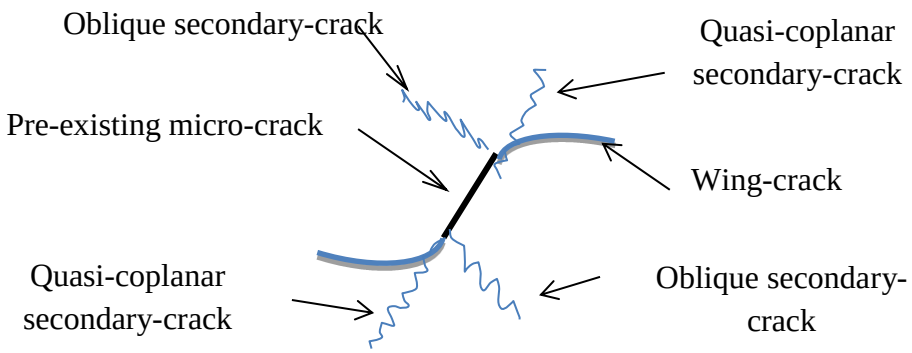

Figure 4. Crack patterns induced in a rock-like specimen containing an inclined-crack subjected to tension.

Also a great number of experiments have been performed on the rock and rock-like specimens with pre-existing micro-cracks under uniaxial compression loadings. Wing-cracks and secondary-cracks have been observed in a large number of these experiments [6].

4. Verification of DDM with quadratic collocation using analytical solution

A simple problem for verifying the numerical results and the proposed code is presented in this paper. This problem is the center slant micro-crack in an infinite specimen, shown in Figure 5. The slant angle φ changes counter-clockwise from the x (horizontal) axis, and the tensile stress σ^{∞} = 10 MPa is acting, considering the two cases parallel to the (i) x-axis and (ii) y-axis. Half of the micro-crack length, b= 1 mm, modulus of elasticity E=10 GPa, Poisson's ratio $\nu = 0.2$, and fracture toughness K_{IC}= 1.8MPa $m^{1/2}$ are assumed. The analytical solution of the mode I and mode II SIFs, k_I and k_{II} for the infinite problem are given as [42]:

$$K_I = \sigma^{\infty}(\pi b)^{\frac{1}{2}}\varpi_i$$
$$K_{II} = \sigma^{\infty}(\pi b)^{\frac{1}{2}}\varpi_{ii} \quad (16)$$

where ϖ_{ii} and ϖ_i are the dimensionless functions; they enter the effects of loading and segment geometry into SIFs, and also must be calculated for any problem.

For example, for the following sample (Figure 5), the functions ϖ_{ii} and ϖ_i in relation (16) can be written as:

$$\varpi_i = \sin^2\varphi$$
$$\varpi_{ii} = \sin^2\varphi.\cos\varphi \quad (17)$$

Here, in order to predict the angle of wing-crack initiation and the extension of micro-crack, the maximum tangential stress criterion has been used. This is a classical mixed mode criterion which has been used vastly by several researches [3, 30, 40- 44]. Based on this criterion, it can be found out that micro-cracks always grow in the perpendicular direction to the maximum tensile stress. The maximum tangential strain stress σ_θ (in the extension of the micro-crack propagation) truly befalls in the following conditions; the micro crack-propagation will initiate.

$$\theta_0 = \frac{1}{\sqrt{2\pi r}}\cos\frac{\theta_0}{2}\left[K_I\sin\frac{\theta_0}{2}\cos\frac{\theta_0}{2} + K_{II}(1-3\sin^2\frac{\theta_0}{2})\right] = 0 \quad (18)$$

Using this equation, the wing-crack initiation angle (θ_0) can be determined:

$$\theta_0 = 2\tan^{-1}\left[\frac{K_I}{4K_{II}} \pm 0.25\sqrt{\frac{K_I^2}{K_{II}^2}+8}\right] for \;\; K_{II} \neq 0, \quad (19)$$
$$\text{and} \;\; \theta_0 = 0 \;\; for \;\; K_{II} = 0$$

Finally, the general form of criterion, σ_θ, in the toughness conditions for the fracture of materials of mode I (i.e., k_{IC}) and wing-crack initiation angle can be expressed as the following relation [36, 40]:

$$\cos\frac{\theta_0}{2}\left[K_I\cos^2\frac{\theta_0}{2} - \frac{3}{2}K_{II}\sin\frac{\theta_0}{2}\right] = K_{IC} \;\; (\text{or } 0.866K_{II}) \quad (20)$$

K_I and θ_0 for different micro-crack inclination angles are obtained analytically using equations (19-20). The linear and quadratic collocation formulations have both been implemented into the DDM code TDDCRACK^{2D} (based on the linear elastic fracture mechanics), and used to numerically solve this example problem. Different micro-crack inclination angles under the tensile stress have been used for the above mentioned cases. There are totally 96 elements including 90 elements along the micro-crack and six elements, three elements for each of the two micro-crack tips. An L/b ratio of 0.1 was used to operate the linear and quadratic collocation displacement discontinuity codes. The results computed by the TDDCRACK^{2D} code for quadratic collocations are given in Table 1, and graphically illustrated in Figures 6 and 7 for the both cases (i) and (ii), respectively, which show the correctness and helpfulness of the quadratic collocation formulation for the behavior of the cracked solids. The results obtained show that the numerical values obtained by the TDDCRACK^{2D} code using quadratic collocation are very accurate compared to those obtained using linear collocation, and are very close to the analytical results. Also, according to Figure 8, wing-crack initiation angle increases with reduction in the value of stress intensity factor.

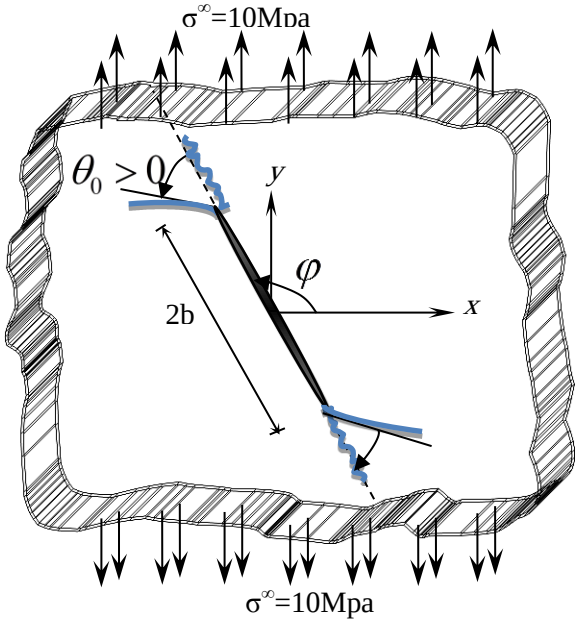

Figure 5. A center slant micro-crack in an infinite body under a uniform tension parallel to the y-axis.

Table 1. Analytical and numerical values for mode I and mode II SIFs $K_I/(\sigma^\infty\sqrt{\pi b})$ and $K_{II}/(\sigma^\infty\sqrt{\pi b})$ for different micro-crack inclination angels, using only 90 quadratic elements (360 collocation points) and three special crack tip elements (L/b=0.1).

φ Angle	LOADING (x-axis)				LOADING (y-axis)			
	$K_I/(\sigma\sqrt{\pi b})$		$K_{\Pi}/(\sigma\sqrt{\pi b})$		$K_I/(\sigma\sqrt{\pi b})$		$K_{\Pi}/(\sigma\sqrt{\pi b})$	
	Analytical	TDDCRACK (quadratic)	Analytical	TDDCRACK (quadratic)	Analytical	TDDCRACK (quadratic)	Analytical	TDDCRACK (quadratic)
170°	0.0301	0.0301	0.171	0.1710	0.9698	0.9699	0.171	0.1710
160°	0.1169	0.1169	0.3213	0.322	0.8830	0.8830	0.3213	0.3214
150°	0.2500	0.25	0.433	0.4377	0.7500	0.7501	0.433	0.433
140°	0.4131	0.4129	0.492	0.4922	0.5868	0.5870	0.492	0.4926
130°	0.5868	0.5869	0.4924	0.4924	0.4131	0.4132	0.4924	0.4924
120°	0.7500	0.7500	0.433	0.4333	0.2500	0.2491	0.433	0.4330
110°	0.8830	0.8830	0.3213	0.3214	0.1169	0.1169	0.3213	0.3221
100°	0.9698	0.9699	0.171	0.1714	0.0301	0.0301	0.171	0.1710

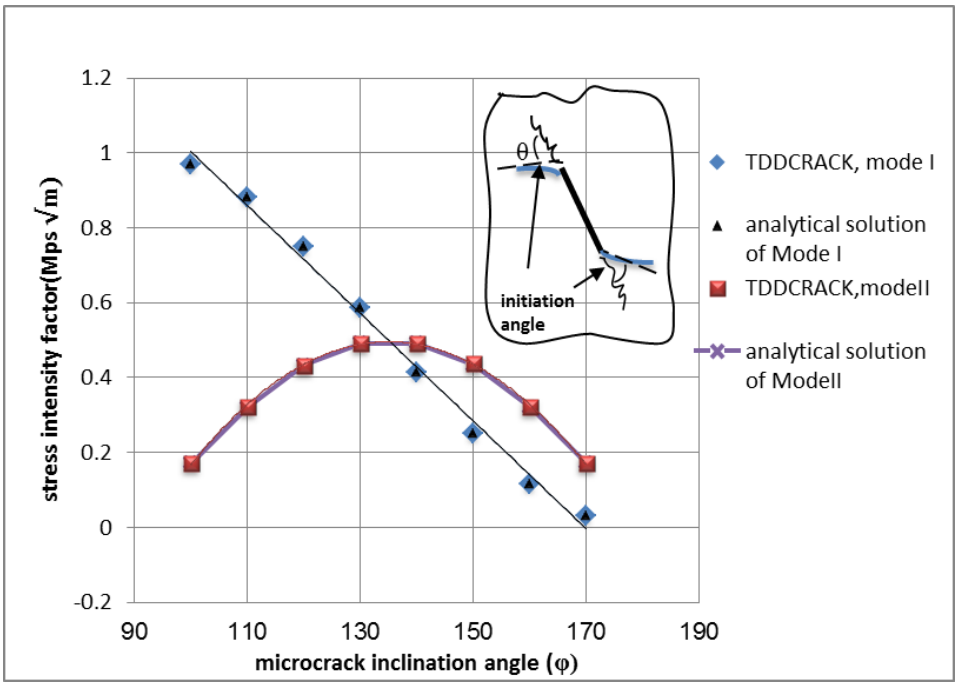

Figure 6. Analytical and numerical values for mode I and mode II stress intensity factors $K_I/(\sigma^{\infty}\sqrt{\pi b})$ and $K_{II}/(\sigma^{\infty}\sqrt{\pi b})$ for inclined single micro-cracks under a uniform tension parallel to x-axis, for L/b=0.1 and 270+6 points of quadratic collocation.

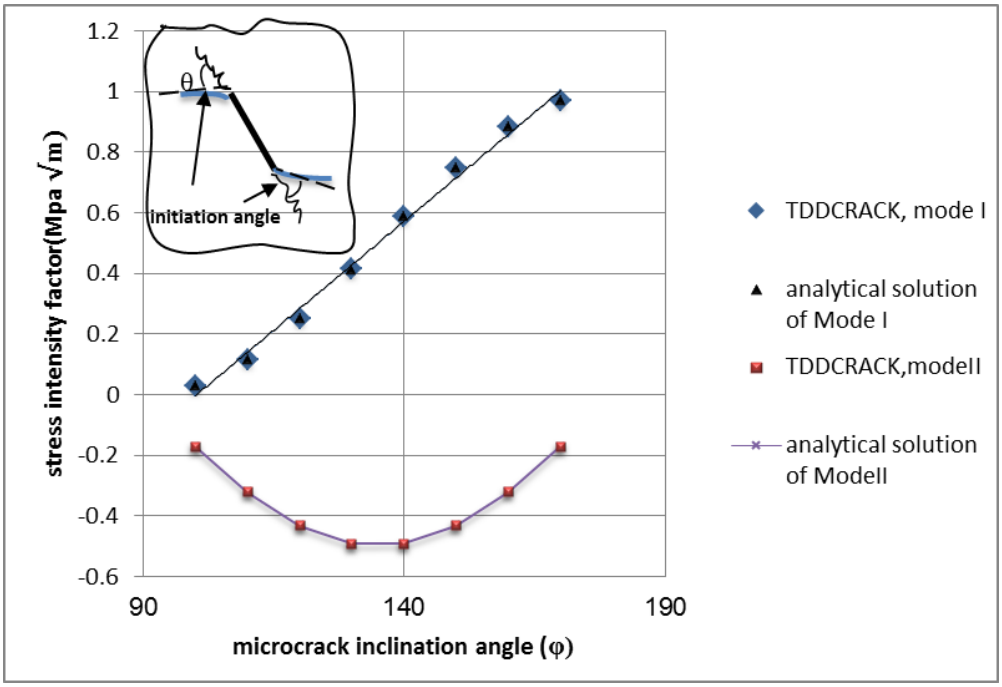

Figure 7. Analytical and numerical values for mode I and mode II SIFs $K_I/(\sigma^{\infty}\sqrt{\pi b})$ and $K_{II}/(\sigma^{\infty}\sqrt{\pi b})$, for inclined single micro-cracks under a uniform tension parallel to y-axis for L/b=0.1 and 270+6 points of quadratic collocation.

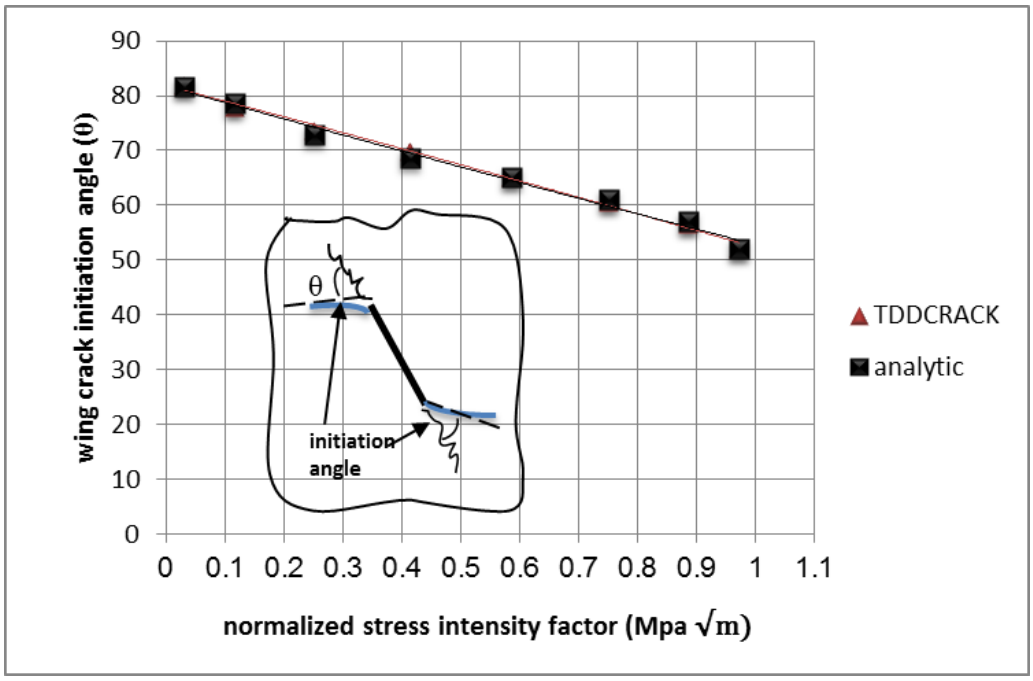

Figure 8. Relationship between stress intensity factor and micro-crack initiation angle.

Figure 8 shows that at low SIFs, micro-crack initiation angles increase.

The center slant micro-crack problem has been solved by different researchers, e.g. Guo et al. [43], to get a simple analysis. These researchers have also used the constant element displacement discontinuity with a special crack tip element for the angles 30, 40, 50,60,70, and 80 degrees. To evaluate the micro-crack initiation angle θ_0, they have used two initiation criteria: maximum tangential tensile stress criterion (σ_θ-criterion) and minimum strain energy density criterion (S-criterion), and compared their results with the results obtained from other models. The results obtained for the micro-crack initiation angle θ_0 by TDDCRACK^{2D}Code from the quadratic collocations using the maximum tangential tensile stress criterion, and the results obtained by Guo et al. [43] are given in Table 2, and graphically illustrated in Figure 9. As it can be seen in this table, the numerical results obtained by the TDDCRACK^{2D}Code are comparatively more accurate.

Table 2. Micro-crack initiation angle θ_0 for center slant micro-crack problem obtained by different methods.

Angle	Results obtained by TDDCRACK$_{2D}$ code		Results obtained by Guo et al [43].		
	Quadratic collocation	σ-criterion	S-criterion	Experimental	Numerical
150°	60.0098°	60.2°	63.5°	62.4°	67.0°
140°	55.65°	55.7°	56.7°	55.1°	59.0°
130°	50.29°	50.2°	49.5°	51.1°	51.0°
120°	43.22°	43.2°	41.9°	43.1°	41.0°
110°	33.26°	33.2°	31.8°	30.7°	29.0°
100°	18.91°	19.3°	18.5°	17.3°	15.0°

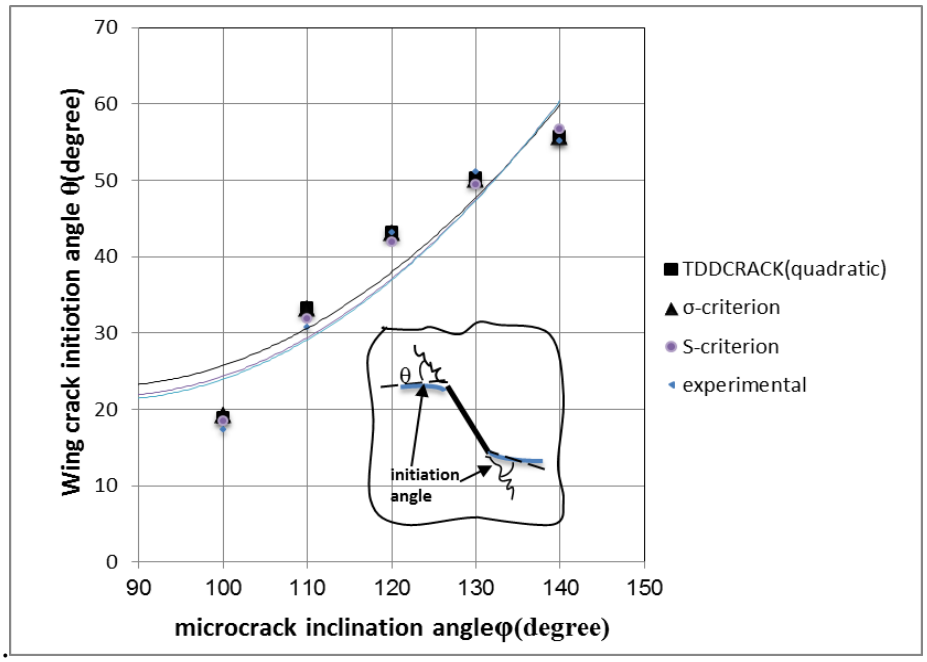

Figure 9. Micro-crack initiation angle θ_0 as a function of micro-crack inclination angle φ.

5. Effects of specimen size and boundary

Consider a center slant micro-crack in a finite plate having a width *2W*, as shown in Figure 10. Let the micro-crack length *b=1*mm, the tensile stress σ= 10 MPa (acting parallel to the y-axis), modulus of elasticity E=10 GPa, Poisson's ratio ν= 0.2, and fracture toughness K_{IC}= 1.8 MPa $m^{1/2}$.

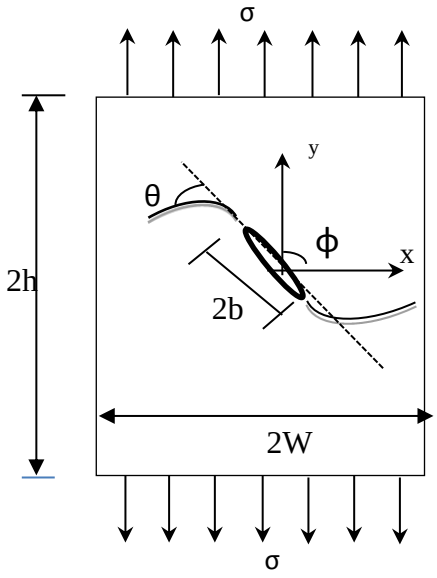

Figure 10. A degree center slant micro-crack in a finite plate with w/h=1.

The effect of specimen boundary on the crack propagation mechanism of a single micro-crack can be studied by considering the micro-crack inclination angles φ as 150°, 135°, and 120°. Table 3 shows the effect of specimen boundary on the normalized values evaluated considering different b/W ratios. The ratio of micro-crack length, b, to plate width, W, changes as $\frac{b}{w} = 0.01, 0.03, 0.06, 0.09, 0.2, 0.4, 0.6, 0.8$.

The normalized SIFs $K_I / (\sigma\sqrt{\pi\, b})$ and $K_{II} /(\sigma\sqrt{\pi b})$ and crack initiation angles (θ) for different micro-crack inclinations are obtained numerically by means of the computer code TDDCRACK[2D].

Table 3. Numerical values for normalized mode I and mode II stress intensity factors $K_I/(\sigma\sqrt{\pi b})$, $K_{II}/(\sigma\sqrt{\pi b})$, and crack initiation angle (θ) for center slant micro-crack, using different crack length to plate width ratios (i.e. different b/W ratios).

b/W	Φ=120°			φ =135°			φ =150°		
	$K_I/(\sigma\sqrt{\pi b})$	$K_{II}/(\sigma\sqrt{\pi b})$	θ	$K_I/(\sigma\sqrt{\pi b})$	$K_{II}/(\sigma\sqrt{\pi b})$	θ	$K_I/(\sigma\sqrt{\pi b})$	$K_{II}/(\sigma\sqrt{\pi b})$	θ
0.01	0.254	0.432	59.79°	0.504	0.498	52.97°	0.753	0.432	43.07°
0.03	0.255	0.432	59.79°	0.504	0.499	52.96°	0.754	0.432	43.07°
0.06	0.255	0.433	59.78°	0.506	0.500	52.95°	0.757	0.433	43.05°
0.09	0.257	0.435	59.76°	0.509	0.502	52.93°	0.761	0.435	43.03°
0.2	0.266	0.446	59.66°	0.529	0.517	52.78°	0.793	0.449	42.84°
0.4	0.306	0.49	59.2°	0.608	0.571	52.16°	0.913	0.498	42.04°
0.6	0.39	0.565	58.08°	0.758	0.661	50.94°	0.986	0.575	40.61°
0.8	0.58	0.676	55.34°	1.024	0.793	48.89°	1.478	0.691	38.78°

The numerical results obtained are illustrated graphically in Figures 11 to 13. The results given in Table 3 and Figures 11 to 13 show that as the b/W ratio increases above 0.4, the normalized SIFs $K_I/(\sigma\sqrt{\pi b})$ and $K_{II}/(\sigma\sqrt{\pi b})$ also increase but for the ratios below 0.4, the SIFs approache their corresponding analytical values for the infinite body case (as expected) [43]. One may find that when the micro-cracks approach the left and right surfaces of the specimen, the SIFs increase, and the propagation of crack slows down.

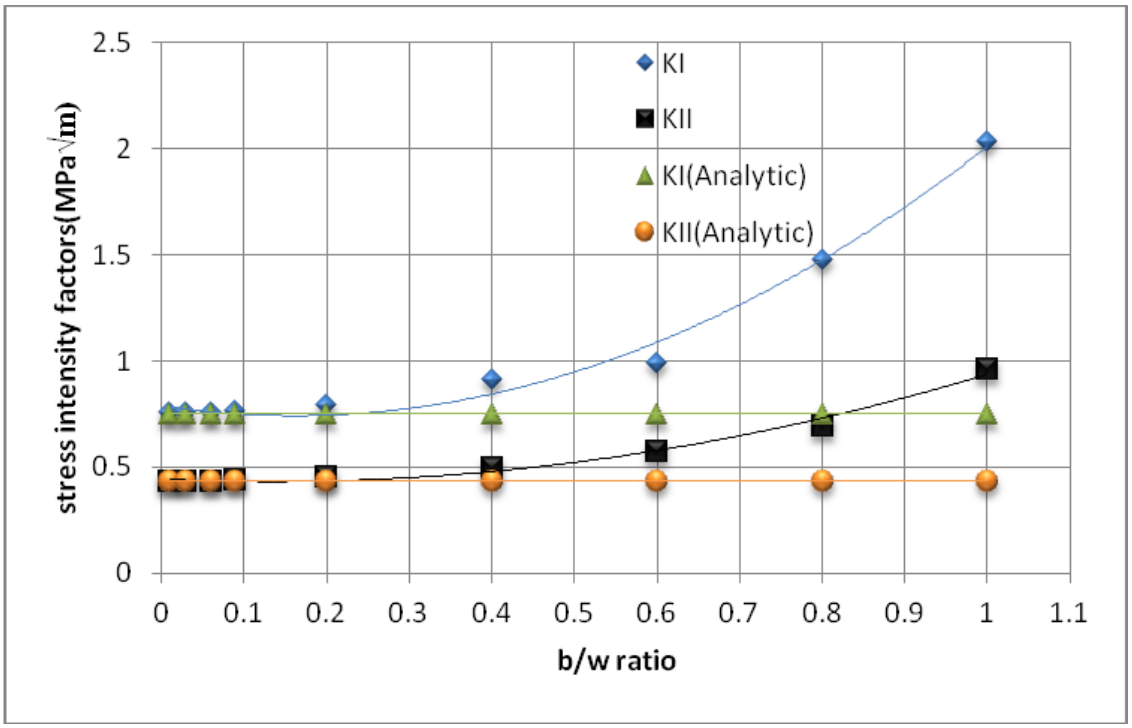

Figure 11. Normalized SIFs $K_I/(\sigma\sqrt{\pi b})$ and $K_{II}/(\sigma\sqrt{\pi b})$ *vs.* different b/W ratios in a finite rock specimen for φ=150°.

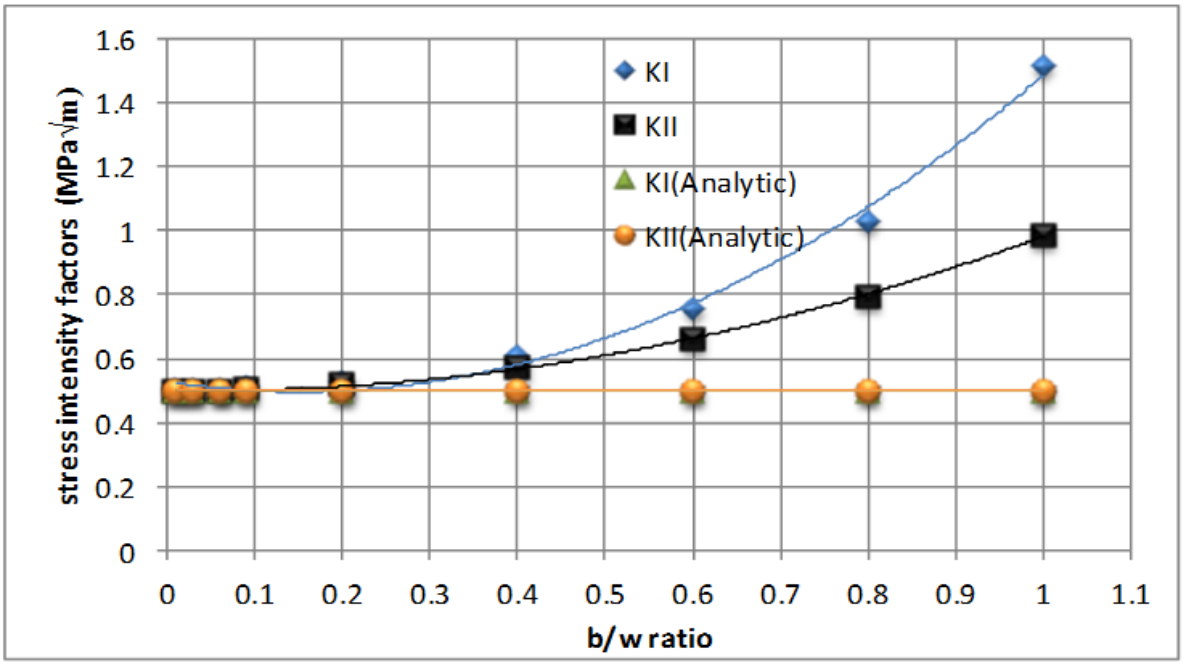

Figure 12. Normalized stress intensity factors $K_I / (\sigma\sqrt{\pi b})$ and $K_{II} /(\sigma\sqrt{\pi b})$ *vs.* different b/W ratios in a finite rock specimen for φ=135°.

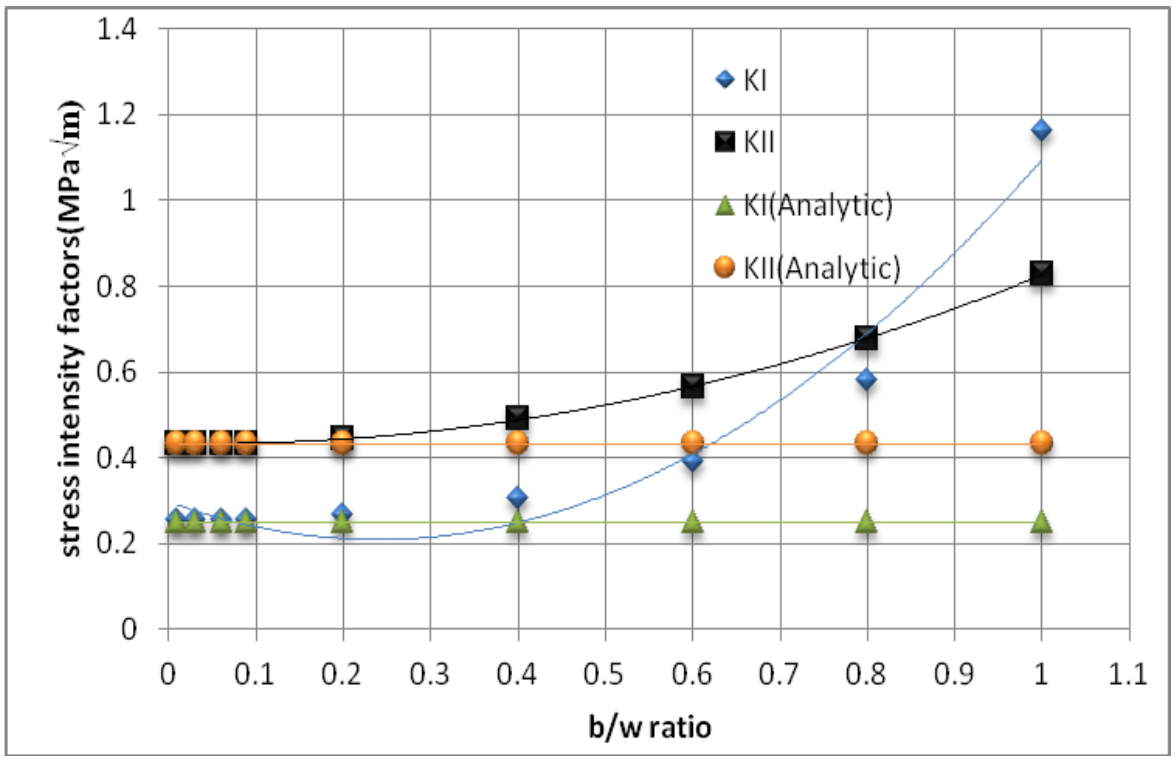

Figure 13. Normalized SIFs $K_I / (\sigma\sqrt{\pi b})$ and $K_{II} /(\sigma\sqrt{\pi b})$ *vs.* different b/W ratios in a finite rock specimen for φ=120°.

6. Initiation and interaction of three pre-existing micro-cracks

6.1. Effects of orientation of micro-cracks on SIFs

Consider a specimen with three micro-cracks, as shown in Figure 14. Two of these micro-cracks are parallel, but the third one is not. The physical and loading parameters are the same as those given for the center slant crack problem, shown in Figure 5 (section 4).

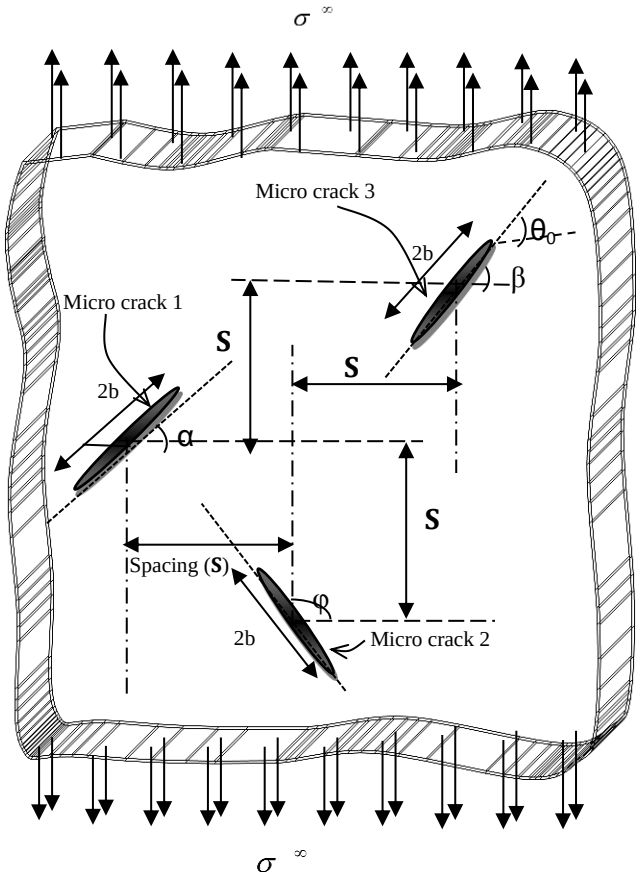

Figure 14. Three inclined micro-cracks in an infinite body under a uniform normal tension with spacing S=2b.

Figures 15 and 16 show the plots of mode I and mode II SIFs for six original tips of micro-cracks by considering micro -crack 1 and micro-crack 3(micro-crack 1 and micro-crack 3 are parallel) with constant inclination angles α=60° and β=60° and the micro-crack 2 are at different ψ angles with respect to the direction of micro-crack 1 and micro-crack 3 (i.e. at angles, φ= 150°, 140°,120°, 100°,80°, and 60°.

The effect of orientation brings about the following properties.

For the original tip4, k_I is always a constant value for different inclination angles of micro-crack3, because in this case, it is in the state of "zero interaction". For the original tip 1, k_I value increases a bit by increasing the inclination angle of micro-crack3 (φ) from 60 to 120, and from 120 to 150, it decreases. For the original tip 2, for k_I value, there is a little increase in the inclination angle for micro-crack3 (φ) from 60 to the vertical, and from this to 150 there is a decrease. For the original tip 3, k_I value shows a small decrease with increase in the inclination angle of micro-crack3 (φ) from 60 to 90, and from 90 to 150, there is a small increase. For the original tip 6, k_I decreases considerably with increase in the inclination angle of micro-crack3 (φ) from 60 to 90, because the maximum interaction of the micro-crack appears to befall for the inclination angle of micro-crack3 that is equal to 150, while micro-crack3 appears to be fully non-oriented with micro-crack 2. In fact, k_I gets the zero value when φ is almost 90, because micro-crack3 is almost 90, since it grows further in the shearing mode. The maximum value for k_I (0.772) befalls

at φ=150 because the original tip 6 strongly interacts with the lower original tip formicro-crack1. As it was previously shown for two micro-cracks, treatment of k_{II} also shows a significant difference in k_I for the three micro-cracks. For the original tips of micro crack3, in the range of 130<φ<140, $|k_{II}|$ increases when micro-crack 1 is completely non-oriented with micro-crack 2. In contrast, when the two original tips of micro-crack3 approach other original tips of the neighboring micro-cracks, both k_I and $|k_{II}|$ increase as the distance between the original tips decreases.

According to Figure 17, the wing-crack initiation angles of all the original tips *vs.* the micro-crack inclination angles change in the inclination angle of micro-crack3, and the inclination angles for other micro-cracks are constant. Based on Figure 17, the most changeability is in the original tips of micro-crack 3. The maximum value for the wing crack initiation angle (θ_0~77) befalls at φ=150 for the original tip5.

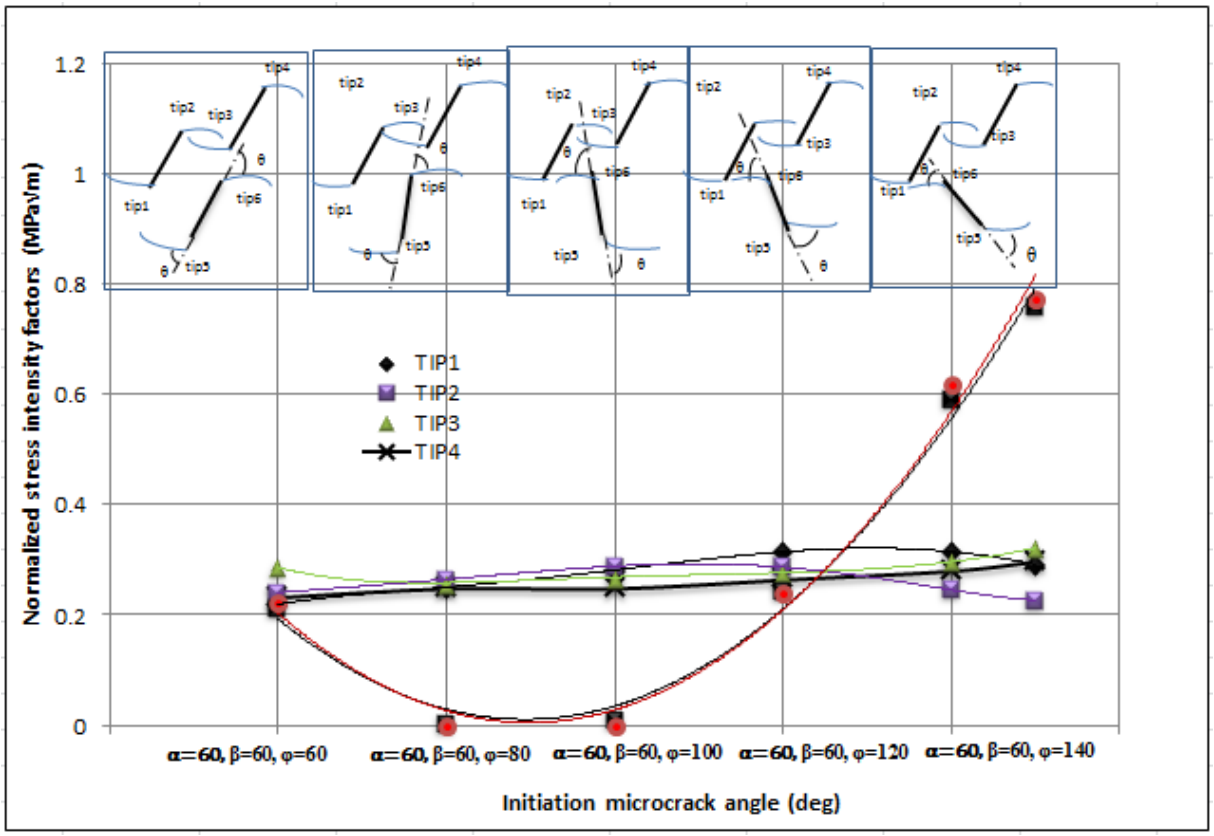

Figure 15. Treatment of mode I SIFs *vs.* locations of three micro-cracksunder a uniform tension parallel to the y-axis for L/b=0.1 and 360+6 points for each micro-crack.

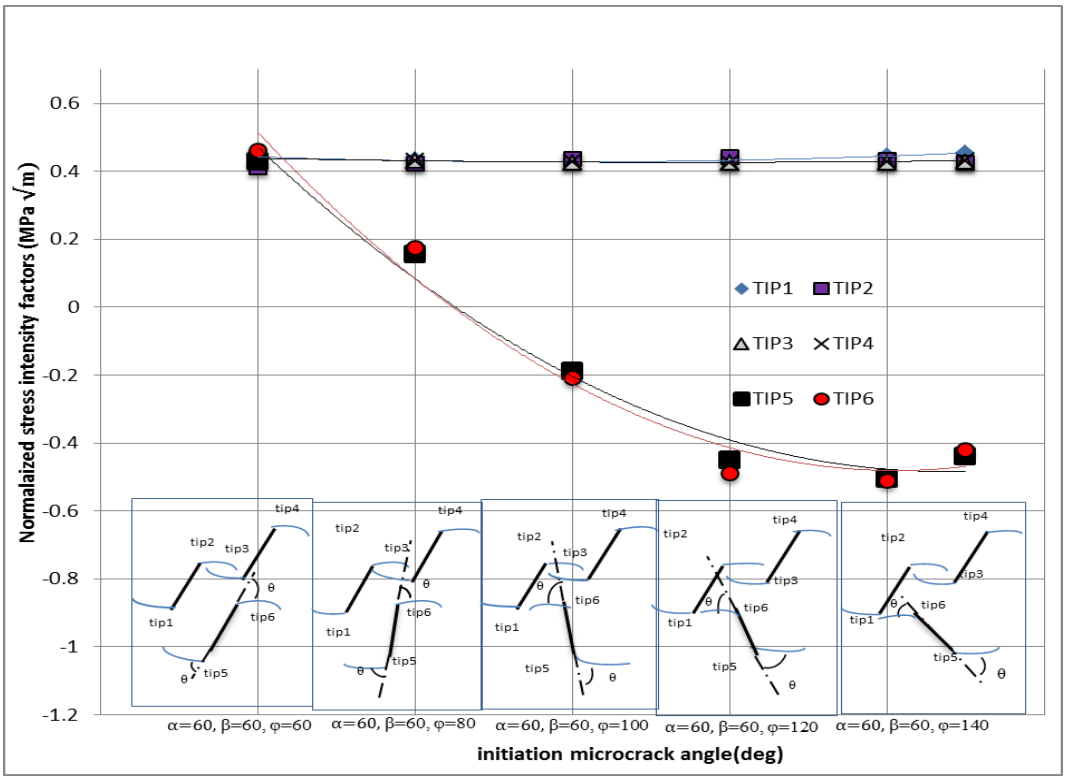

Figure 16. Treatment of mode II SIFs *vs.* locations of three micro-cracks under a uniform tension parallel to y-axis for L/b=0.1 and 360+3 points for each micro-crack.

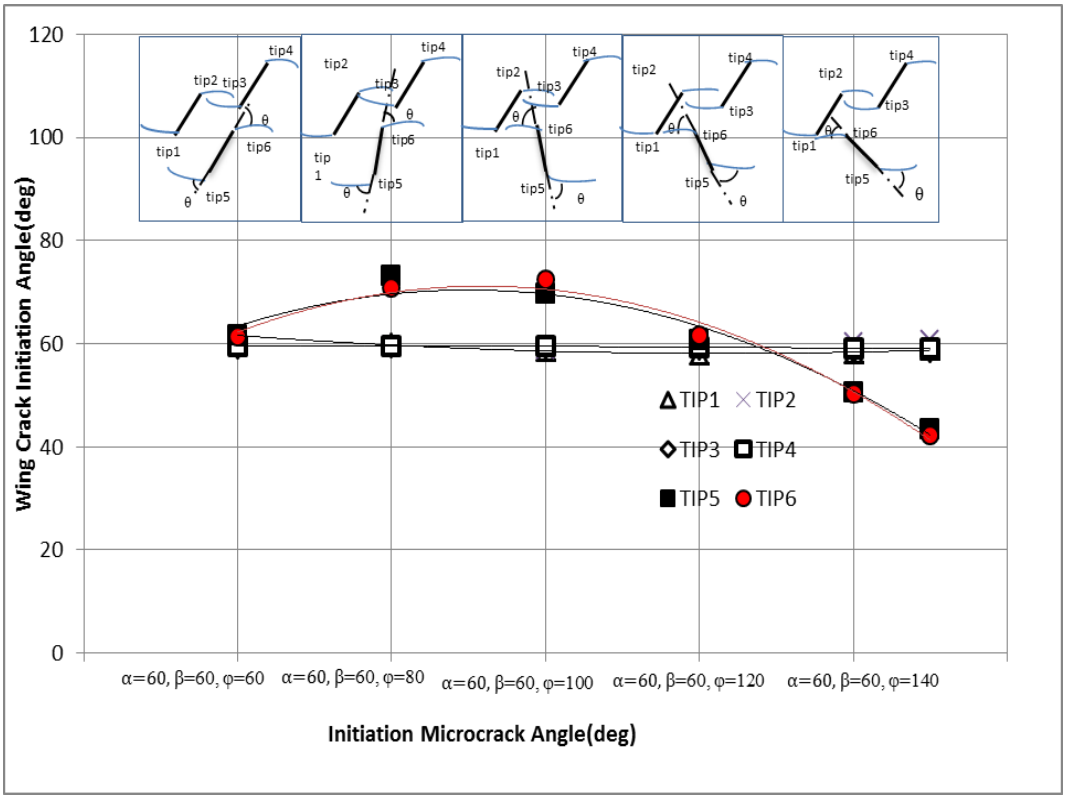

Figure 17. Wing crack initiation angle *vs.* locations of three micro-cracks under a uniform tension parallel to y-axis for L/b=0.1 and 360+3 points for each micro-crack.

6.2. Treatment of SIFs on distances of three micro-cracks from each other

Any original micro-crack tip has a zone of stress influence. In this zone, the linear elastic fracture mechanics (LEFM) theory is used to obtain linear elastic solutions [12, 32]. If the zones of the influence of stress resulted from each micro-crack are far enough from each other, they act as a single micro-crack in the computation of SIFs for each original tip (i.e. there is zero interaction). Figure 18 shows the zone stress influence for a single micro-crack.

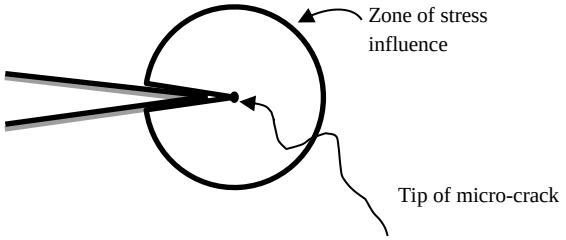

Figure 18. Zone of stress influence for a single micro-crack.

In the present study, each one of the three micro-cracks present has vertical and horizontal distances in its own center to those of the other micro-cracks. For any of the three micro-cracks, the main micro-crack orientation is α=60, β=50, and φ=40, and the main micro-crack lengthis 2*b* in this example. As it is shown in Figures 19 and 20, the mode I and mode II SIFs are changed by varying *S*. The mode I and mode II SIFs are changed in different spacings. The mode I and mode II SIFs for five different spacings were obtained (for *S/b*= 1, 1.5, 2, 2.5, 3). The results obtained show that with increase in the spacing, k_I and k_{II} are likely to reach the value for zero interaction when the micro-cracks get much far away from each other (i.e. for large S and/or S/b ratios). In fact, for the original tip 6, k_I gets the zero value if *S*<1. Hence, the wing crack propagated length from the original tip 6 is likely to be limited since wing-crack cannot grow towards the center of the micro-crack (See Figure 19). The maximum value for k_I (0.65) befalls when *S*= 1 because the original tip 6 strongly interacts with the lower original tip of micro-crack1. As increases more and more, k_I tends toward the value for zero interaction, i.e. for the original tips 4 and 5. Figure 20 shows the mode II stress intensity factor with respect to different spacings for completely non-oriented micro-cracks. The figure shows that mode II SIFs of the original tips 1 and 2 for micro-crack 3 are negative in comparison with the other original tips of micro-cracks. Figure 21 shows the wing-crack initiation angles of all original tips, that changed in spacing.

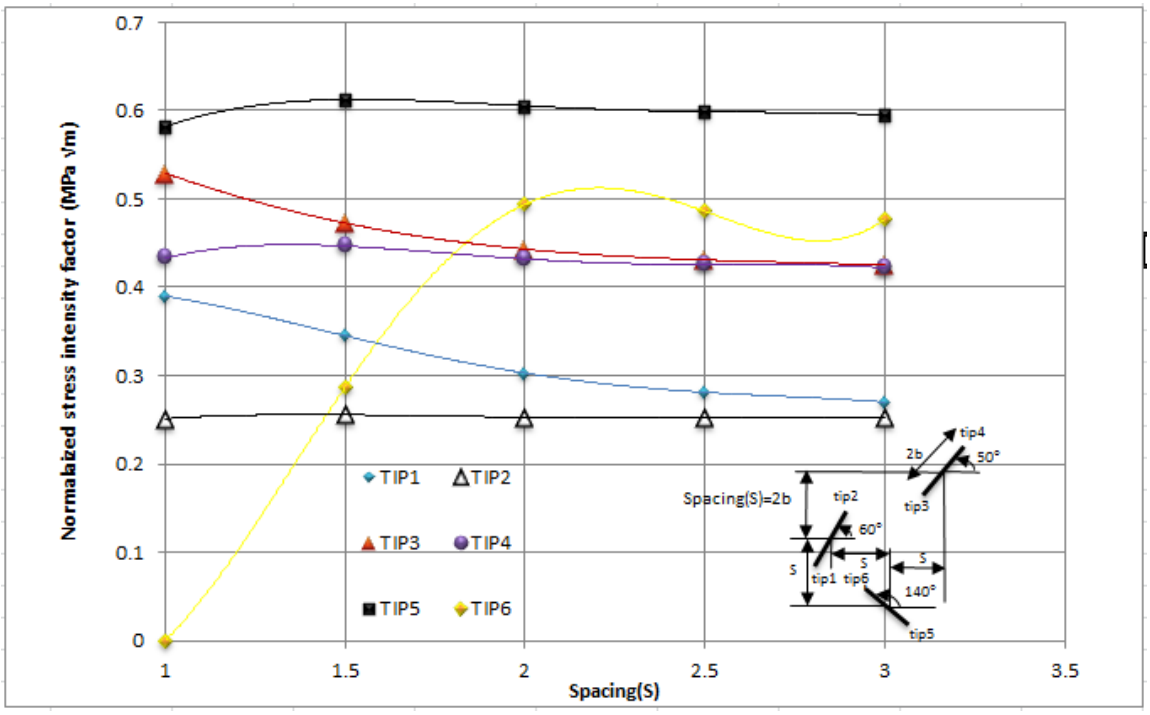

Figure 19. Treatment of mode I SIFs *vs.* distance S for three micro-cracks. (parameter *S* represents the distance of the center of any micro-crack with respect to horizontal and vertical axes).

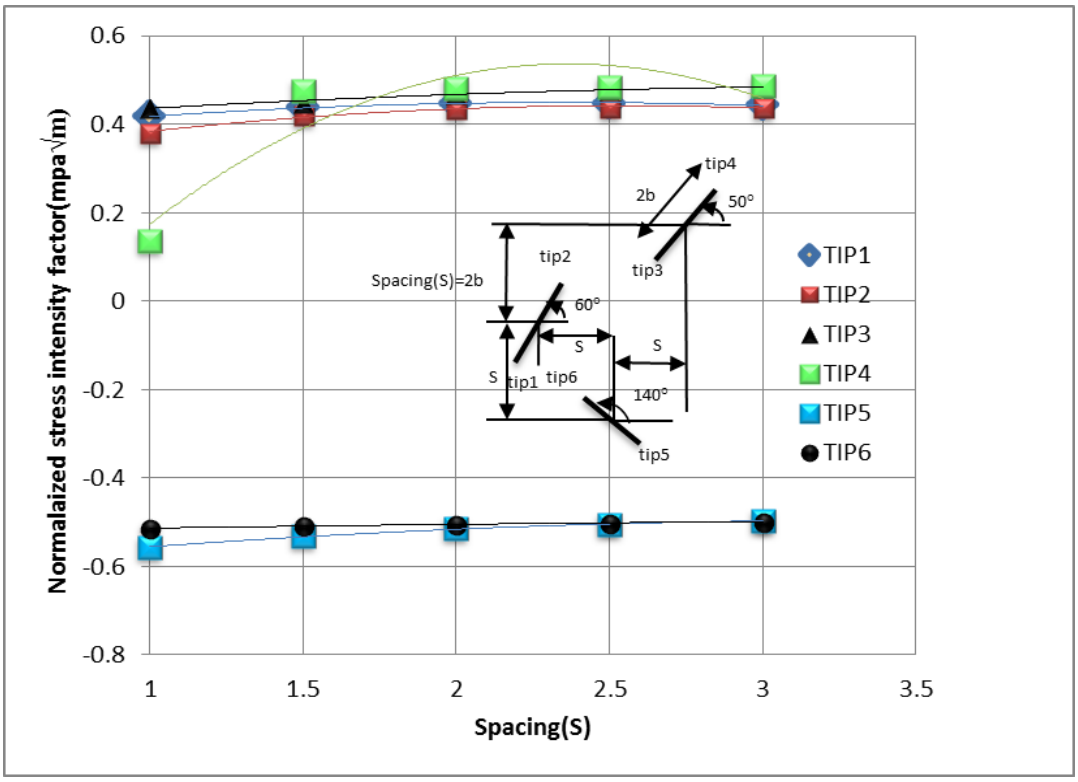

Figure 20. Treatment of mode II SIFs *vs* .distance S for three micro-cracks. (parameter *S* represents distance of center of any micro-crack with respect to horizontal and vertical axes).

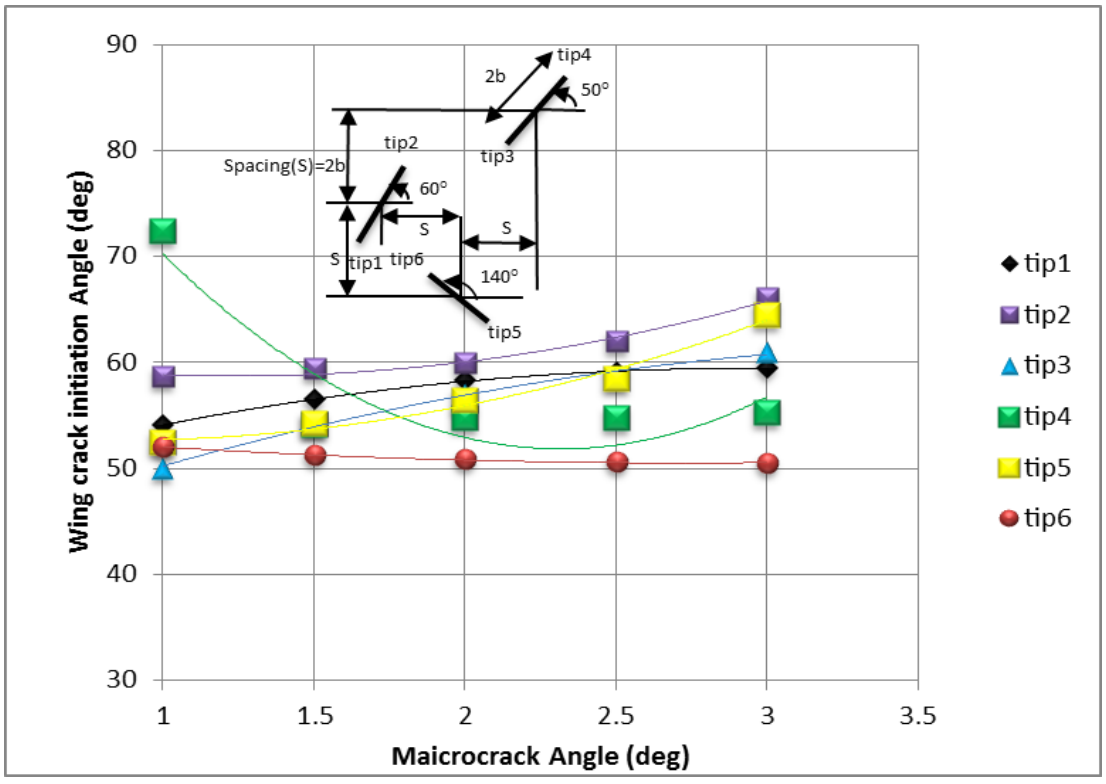

Figure 21. Wing-crack initiation angle *vs.* distance S for three coalescing micro-cracks. (parameter *S* represents distance of center of any micro-crack with respect to horizontal and vertical axes).

7. Conclusions

According to the complexity of crack coalescence problem, accurate calculation of SIFs related to micro-cracks and interactions of all micro-cracks with each other using micro-mechanics discrete methods and finite element analysis (FEM) are, to some extent, difficult or time-consuming. Therefore, semi-analytical methods like the displacement discontinuity method (DDM), based on the linear elastic fracture mechanics (LEFM) theory, can be used. A numerical model on the basis of computing the stress intensity factors (SIFs) and wing-crack initiation angles for cracked substances under a normal uniform tension was presented. Any mixed mode fracture criterion can be implemented to this numerical code. However, in the present work, based on the LEFM principles, the maximum tangential stress criterion or σ-criterion was implemented into the Code TDDCRACK^{2D}in order to investigate the interactions of micro-cracks. TDDCRACK^{2D} is a well-organized and -verified computer code. The structure of this code is segmental, and considers two boundary conditions for each micro-crack. Several simple and frequently used samples could be selected and explained to verify the present numerical method. However, here, it was limited to only one. Also to show that the results are in a good agreement with the analytical solutions and experimental observations for single micro-cracks, in these models, linear and quadratic collocations with three special crack tip elements for each micro-crack tip at the same time were implemented into the Code TDDCRACK^{2D}. The differences between parallel micro-cracks and non-oriented micro-cracks were further discovered using the mentioned numerical method. The numerical simulation was carried out considering infinite planes with three micro-cracks under a uniform tension.

Studied variables:

Comparing the parallel and non-parallel micro-cracks, the effects of crack distances and inclinations of three micro-cracks showed that these factors had a strong influence on the breaking path. However, this model is capable of solving problems in the fractured media containing multiple micro-cracks under various loading conditions, e.g. pure tensile, pure shear, and tension shear.

Acknowledgment

This work is sponsored by Iran's National Elites Foundation (INEF). Partial supports of center of excellent for structures and earthquake engineering at Sharif University of Technology is greatly appreciated.

References

[1]. Golshani, A., Okui, y., oda, m. and takemura, t. (2005). Micromechanical model for brittle failure of rock and its relation to crack growth observed in triaxial compression tests of granite.Int. J. Mechanics of Materials 38:287-303.

[2]. Niu, J. and S. WU. MAO. (1998). Analysis of asymmetric kinked cracks of arbitrary size, location and orientation – Part I. Remote compression. Int. J. Frac. 89: 19–57.

[3]. Marji, M. F. and Dehghani, I. (2010). Kinked crack analysis by a hybridized boundary element/boundary collocation method. Int. J Solids and Structures 47: 922–933.

[4]. Li, t. and Yang, W. (2001). Expected coalescing length of displacement loading collinear micro cracks. Theoret. Appl. fracture mechanics 36: 17-21.

[5]. Hoek, E. and Bieniawski, Z.T. (1965). Brittle Rock Fracture Propagation in Rock under Compression, South African Council for Scientific and Industrial Research Pretoria. Int. J. Frac. Mech. 3: 137-155.

[6]. Park, C. H. (2008). Coalescence of Frictional Fractures in Rock Materials, PhD Thesis, Purdue University West Lafayette, Indiana.

[7]. Haeri, H., Shahriar, K., Marji, M. F. and Moaref Vand, P. (2013). Modeling the Propagation Mechanism of Two Random Micro cracks in Rock Samples under Uniform Tensile Loading, in: Proceedings of 13th International Conference on Fracture, China.

[8]. Horii, H. and Nemat-Nasser, S. (1985). Compression-Induced Micro crack Growth in Brittle Solids: Axial Splitting and Shear Failure. Journal of Geophysical Research, 90: 3105-3125.

[9]. Wong, R.H. and Chau, K.T. (1998). Crack Coalescence in a Rock-like Material Containing Two Cracks, Int. J. Rock mech. and Min. Sci. 35: 147-164.

[10]. Reyes, O. and Einstein, H.H. (1991). Failure Mechanism of Fractured Rock- A Fracture Coalescence Model, Proceedings 7th International Congress of Rock Mechanics 1: 333-340.

[11]. Shen, B., Stephansson, O., Einstein, H.H. and Ghahreman, B. (1995). Coalescence of fractures under shear stress experiments. Journal of Geophysical Research. 100: 5975-5990.

[12]. Bobet, A. and Einstein, H.H. (1998 a). Fracture Coalescence in Rock-type Materials under Uniaxial and Biaxial Compression. Int. J. Rock Mech and Min. Sci. 35: 863-888.

[13]. Bobet, A. and Einstein, H.H. (1998 b). Numerical Modeling of Fracture Coalescence in a Model Rock Material. Int. J. Frac. 92: 221-252.

[14]. Vásárhelyi, B. and Bobet, A. (2000). modeling of crack initiation, propagation and coalescence in uniaxial compression, Eng. Fract.e Mech. 66: 187-219.

[15]. Wong, R. H. C., Chau, K. T., Tang, C. A. and Lin, P. (2001). Analysis of crack coalescence in rock-like materials containing three flaws – Part I: experimental approach. Int. J. Rock Mech and Min. Sci. 38: 909-924.

[16]. Sagong, M. and Bobet, A. (2002). Coalescence of multiple flaws in a rock-model material in uniaxial compression, Rock Mechanics and Mining Sciences, 39: 229-241.

[17]. Li, Y. P., Chen, L .Z. and Wang, Y. H. (2005). Experimental research on pre-cracked marble under compression. Int.J. Solids and Structures. 42: 2505-2516.

[18]. Ko, T. Y., Einstein, H. H. and Kemeny, J. (2006). Crack Coalescence in Brittle Material under Cyclic Loading, Golden Rocks, 41st U.S. Symposium on Rock Mechanics (USRMS), ARMA/USRMS, 06-930.

[19]. Wong, L. N. Y. and Einstein, H. H. (2006). Fracturing Behavior of Prismatic Specimens Containing Single Flaws, Golden Rocks, 41st U.S. Symposium on Rock Mechanics (USRMS), 50 Years of Rock Mechanics-Landmarks and Future Challenges, Golden, Colorado, ARMA/USRMS 06-899.

[20]. Lee, H. and Jeon, S. (2011). An experimental and numerical study of fracture coalescence in pre-cracked specimens under uniaxial compression. Int. J. Solids and Structures. 48: 979–999.

[21]. Marji, M. F., Gholamnejad, J. and Eghbal, M. (2011). On the crack propagation mechanism of brittle rocks under various loading conditions. Proceedings of International Multidisciplinary Scientific Geo. Conference. Bulgaria. 561-568.

[22]. Marji, M. F. (2014). Numerical analysis of quasi-static crack branching in brittle solids by a modified displacement discontinuity method. Int. J. Solids and Structures 51:1716–1736.

[23]. Tang, C. A., Tham, L. G., Lee, P. K. K., Tsui, Y. and Liu, H. (2000). Numerical tests on micro–macro relationship of rock failure under uniaxial compression. II. Constraint. Slenderness and size effects. Int J Rock Mech Min Sci. 37: 570–7.

[24]. Zhang, X. P. and Wong, L. N. Y. (2011). Cracking processes in rock-like material containing a single flaw under uniaxial compression: A numerical study based on parallel bonded-particle model approach. Rock Mech. and Rock Eng. 45: 711–737.

[25]. Manouchehrian, A. and Marji, M. F. (2012). Numerical analysis of confinement effect on crack propagation mechanism from a flaw in a pre-cracked rock under compression. Acta Mechanica Sinica. 28: 1389–1397.

[26]. Chan, H. C. M. (1986). Automatic Two-dimensional Multi-fracture Propagation Modelling of Brittle Solids with Particular Application to Rock. Sc. D. Thesis. Massachusetts Institute of Technology. Cambridge, USA.

[27]. Chan, H. C. M., Li, V. and Einstein, H. H. (1990). A hybridized displacement discontinuity and indirect boundary element method to model fracture propagation. Int. J. Fract. 45: 263-282.

[28]. Tang, C. A. and Kou, S. Q. (1998). Crack Propagation and Coalescence in Brittle Materials Under Compression. Eng. Fract. Mech. 61: 311-324.

[29]. Liu, H. Y., Kou, S. Q., Lindqvist, P. A. and Tang, C. A. (2004). Numerical Simulation of Shear Fracture (ModeII) in Heterogeneous Brittle rock. Int. J.Rock mech. Min.sci. 41.

[30]. Ingraffea, A. R. (1983). Numerical Modeling of Fracture Propagation. Rock Fracture Mechanics. Rossmanith H. P. (Ed.). Springer Verlagwien. New York, pp. 151-208.

[31]. Melin, S. (1986). When does a crack grow under mode II condition? International Journal of Fracture. 30:103-114.

[32]. Broek, D. (1989). The Practical Use of Fracture Mechanics, 4th Edition. Kluwer Academic Publishers. Netherland.70. Whittaker BN, Singh RN, Sun G. Rock fracture mechanics: Principles. design and applications. Amsterdam. Elsevier.

[33]. Whittaker, B. N., Singh, R. N. and Sun, G. (1992). Rock fracture mechanics. Principles, design and applications. Amsterdam. Elsevier.

[34]. Shao, J. F. and Rudnicki, J. W. (2000). A micro crack-based continuous damage model for brittle geomaterials. Mechanics of Materials. 32: 607-619.

[35]. Bremaecker, D.E. J-C., Ferris, M. C. and Ralph, D. (2000). Compressional fractures considered as contact problems and mixed complementarity problems. Eng. Fract. Mech. 66: 287-303.

[36]. Chang, Jun., Jin-quan, Xu. and Mutoh, Y. (2006). A general mixed-mode brittle fracture criterion for cracked materials. Engineering Fracture Mechanics. 73: 1249–1263.

[37]. Crouch, S. L. (1976). Solution of Plane Elasticity Problems by the Displacement Discontinuity Method. Int. j. Numer. Meth. Engng. 10: 301-343.

[38]. Crouch, S. L. and Starfield, A. M. (1983). Boundary Element Methods in Solid Mechanics, Allen and Unwin, London.

[39]. Shou, K. J. and Crouch, S. L. (1995). A Higher Order Displacement Discontinuity Method for Analysis

of Crack Problems. Int. J. Rock Mech. Min. Sci. and Geomech. Abstr. 32: 49-55.

[40]. Marji, M. F., Hosseinin_Nasab, H. and Kohsary, A. H. (2006). On the Uses of Special Crack Tip Elements in Numerical Rock Fracture Mechanics. Int. j Solids and Structures. 43: 1669-1692.

[41]. Aliabadi, M. H. (1999). Fracture of Rocks. Computational Mechanics Publications. Southampton. UK.

[42]. Scavia, C. (1990). Fracture Mechanics Approach to Stability Analysis of Crack Slopes. Engng. Fract. Mech. 35: 889-910.

[43]. Guo, H., Aziz, N. I. and Schmidt, L. C. (1990). Linear Elastic Crack Tip Modeling by Displacement Discontinuity Method. Eng. Fract. Mech. 36: 933-943.

[44]. Haeri, H., Shahriar, K., Marji, M. F. and Moaref Vand, P. (2013).Simulating the Bluntness of TBM Disc Cutters in Rocks using Displacement Discontinuity Method, in: Proceedings of 13th International Conference on Fracture, China.

APPENDIX
INTEGRALS AND DERIVATIVES FOR CONSTANT, LINEAR, AND QUADRATIC VARIATIONS OF DISPLACEMENT DISCONTINUITY

1. Constant Integral I_0 and Its Derivatives

$$I_0 = \int_{-c}^{c} \ln\left[(x-\zeta)^2 + y^2\right]^{\frac{1}{2}} d\zeta = y(\theta_1 - \theta_2) - (x-c)\ln(\Gamma_1) + (x+c)\ln(\Gamma_2) - 2c$$

$$I_{0,x} = \frac{\partial I_0}{\partial x} = \ln\Gamma_1 - \ln\Gamma_2$$

$$I_{0,y} = \theta_1 - \theta_2$$

$$I_{0,xy} = -\left(\frac{y}{\Gamma_1^2} - \frac{y}{\Gamma_2^2}\right)$$

$$I_{0,xx} = -\left(\frac{(x-c)}{\Gamma_1^2} - \frac{(x+c)}{\Gamma_2^2}\right) = -I_{0,yy}$$

$$I_{0,xyy} = -\left(\frac{(x-c)^2 - y^2}{\Gamma_1^4} - \frac{(x+c)^2 - y^2}{\Gamma_2^4}\right) = -I_{0,xxx}$$

2. Linear Integral I_1 and Its Derivatives

$$I_1 = \int_{-c}^{c} \zeta \ln\left[(x-\zeta)^2 + y^2\right]^{\frac{1}{2}} d\zeta = xy(\theta_1 - \theta_2) + 0.5(y^2 - x^2 + c^2)\left[\ln(\Gamma_1) - \ln(\Gamma_2)\right] - cx$$

$$I_{1,x} = \frac{\partial I_1}{\partial x} = y(\theta_1 - \theta_2) - x(\ln\Gamma_1 - \ln\Gamma_2)$$

$$I_{1,y} = x(\theta_1 - \theta_2) + y(\ln\Gamma_1 - \ln\Gamma_2)$$

$$I_{1,xy} = (\theta_1 - \theta_2) - c\left(\frac{y}{\Gamma_1^2} + \frac{y}{\Gamma_2^2}\right)$$

$$I_{1,xx} = -\left[\ln\frac{\Gamma_1}{\Gamma_2} + \frac{c(x-c)}{\Gamma_1^2} + \frac{c(x+c)}{\Gamma_2^2}\right] = -I_{1,yy}$$

$$I_{1,xyy} = \frac{x}{\Gamma_1^2} - \frac{x}{\Gamma_2^2} - 2c\left[\frac{(x-c)^2}{\Gamma_1^4} + \frac{(x+c)^2}{\Gamma_2^4}\right]$$

3. Quadratic Integral I_2 and Its Derivatives

$$I_2 = \int_{-c}^{c} \zeta^2 \ln\left[(x-\zeta)^2 + y^2\right]^{\frac{1}{2}} d\zeta = \frac{y}{3}(3x^2 - y^2)(\theta_1 - \theta_2) + \frac{1}{3}(3xy^2 - x^3 + c^3)\ln(\Gamma_1) -$$

$$\frac{1}{3}(3xy^2 - x^3 - c^3)\ln(\Gamma_2) - \frac{2c}{3}(x^2 - y^2 + \frac{c^2}{3})$$

$$I_{2,x} = \frac{\partial I_{21}}{\partial x} = 2xy(\theta_1 - \theta_2) + (y^2 - x^2)(\ln\Gamma_1 - \ln\Gamma_2) - 2cx$$

$$I_{2,y} = (x^2 - y^2)(\theta_1 - \theta_2) + 2xy(\ln\Gamma_1 - \ln\Gamma_2) + 2cy$$

$$I_{2,xy} = 2x(\theta_1 - \theta_2) + 2y\ln\frac{\Gamma_1}{\Gamma_2} - c^2\left(\frac{y}{\Gamma_1^2} + \frac{y}{\Gamma_2^2}\right)$$

$$I_{2,xx} = 2y(\theta_1 - \theta_2) - 2x\ln\frac{\Gamma_1}{\Gamma_2} - c^2\left[\frac{(x-c)}{\Gamma_1^2} + \frac{(x+c)}{\Gamma_2^2}\right] - 4c = -I_{2,yy}$$

$$I_{2,xyy} = 2\ln\frac{\Gamma_1}{\Gamma_2} + c\left[\frac{2x-c}{\Gamma_1^2} + \frac{2x+c}{\Gamma_2^2}\right] - 2c^2\left[\frac{(x-c)^2}{\Gamma_1^4} + \frac{(x+c)^2}{\Gamma_2^4}\right]$$

تحلیل المان مرزی مکانیسم انتشار میکرو ترک‌ها در نمونه‌های شبه سنگی تحت کشش نرمال یکنواخت

هادی حائری[1*]، علیرضا خالو[2]، کوروش شهریار[3]، محمد فاتحی مرجی[4] و پرویز معارف‌وند[3]

۱- پژوهشگر پسا دکتری، دانشکده مهندسی عمران، دانشگاه صنعتی شریف، ایران

۲- دانشکده مهندسی عمران، دانشگاه صنعتی شریف، ایران

۳- دانشکده معدن و متالوژی، دانشگاه امیرکبیر، ایران

۴- دانشکده معدن و متالوژی، دانشگاه یزد، ایران

ارسال ۲۰۱۳/۸/۳، پذیرش ۲۰۱۵/۲/۲۲

* نویسنده مسئول مکاتبات: haerihadi@gmail.com

چکیده:

در این مقاله مکانیسم شکست مواد ترد از قبیل سنگ‌ها تحت بارگذاری کششی نرمال تحلیل شده است. میکرو ترک‌ها معمولاً در تمام مواد پلی کریستالین ناشی از تمرکز تنش ایجاد می‌شوند. مقاله حاضر، ارتباط میکرو ترک‌های از پیش موجود که در نمونه‌های شبه سنگی رشد و انتشار پیدا می‌کنند، مورد توجه قرار داده است. در این مقاله، برنامه کامپیوتری $TDDCRACK^{2D}$ که بر اساس روش ناپیوستگی جابجایی که یکی از زیرمجموعه‌های روش المان مرزی است و بر اصول مکانیک شکست الاستیک خطی بنیان نهاده شده است، استفاده شده است. در این شبیه‌سازی از المان‌های ناپیوستگی جابجایی با مرتبه بالا و از المان‌های مخصوص نوک ترک جهت تخمین فاکتورهای شدت تنش و زاویه شروع ترک‌های باله‌ای برای زوایای مختلف میکرو ترک‌های از پیش موجود داخل یک نمونه بی‌نهایت تحت کشش یکنواخت استفاده شده است.

کلمات کلیدی: میکرو ترک‌ها، ارتباط ترک، شروع ترک، نمونه‌های شبه سنگی، تئوری مکانیک شکست الاستیک خطی، روش ناپیوستگی جابجایی، به‌هم‌پیوستگی ترک.